Letter

Exploring the compactness of α clusters in ^{16}O nuclei with relativistic ^{16}O + ^{16}O collisions

Yuanyuan Wang,[1] Shujun Zhao,[1] Boxing Cao,[1] Hao-jie Xu,[2,3,*] and Huichao Song[1,4,5,†]
[1]*School of Physics, Peking University, Beijing 100871, China*
[2]*School of Science, Huzhou University, Huzhou, Zhejiang 313000, China*
[3]*Strong-Coupling Physics International Research Laboratory (SPiRL), Huzhou University, Huzhou, Zhejiang 313000, China*
[4]*Collaborative Innovation Center of Quantum Matter, Beijing 100871, China*
[5]*Center for High Energy Physics, Peking University, Beijing 100871, China*

(Received 28 January 2024; accepted 16 April 2024; published 7 May 2024)

Probing the α cluster of ^{16}O with the relativistic ^{16}O + ^{16}O collisions has raised great interest in the heavy ion community. However, the effects of the α cluster on the soft hadron observables vary largely among different studies. In this paper, we explain the differences by the compactness of the α cluster in oxygen, using `iEBE-VISHNU` hydrodynamic simulations with different initial state α cluster configurations. We also find several observables, such as the intensive skewness of the $[p_T]$ correlator Γ_{p_T}, the harmonic flows $v_2\{2\}$, $v_2\{4\}$, $v_3\{2\}$, and the $v_n^2 - \delta[p_T]$ correlations $\rho(v_2^2, [p_T])$, $\rho(v_3^2, [p_T])$ in ^{16}O + ^{16}O collisions are sensitive to the compactness of the α cluster in the colliding nuclei, which can be used to constrain the configurations of ^{16}O in the future. Our study serves as an important step toward the quantitative exploration of the α cluster configuration in the light nuclei with relativistic heavy ion collisions.

DOI: 10.1103/PhysRevC.109.L051904

Introduction. The configurations of α clusters in nuclei have attracted much attention from researchers for almost 100 years since the idea was first proposed by Gamow [1]. In particular, the triangular configurations in ^{12}C and the tetrahedral configurations in ^{16}O have been extensively discussed for decades [2–12]. Various approaches have been proposed to study these configurations in both the ground and excited states of the nucleus [13–20]. One of the most interesting approaches is the relativistic heavy ion collisions, where the structure information of the colliding nuclei is imprinted in the created quark-gluon plasma (QGP) [21–35]. The original idea was to collide a light nucleus against a heavy nucleus at high energies to constrain the α cluster configurations of the light nucleus [21]. Recently, both the BNL Relativistic Heavy Ion Collider (RHIC) and the CERN Large Hadron Collider (LHC) have performed or have decided to perform ^{16}O + ^{16}O collisions at high energies [32,36], providing opportunities to probe the α cluster configurations in a heavy ion experiment.

In relativistic heavy ion collisions, the nuclei pass each other in a very short time. The spatial distribution of the colliding nuclei is recorded instantaneously in the initial stage of QGP, which leaves messages in the final state correlations of the emitted hadrons. Since the dynamic evolution of the QGP medium can be well described by relativistic hydrodynamics or transport approaches, the final state observables could be used to study the size and shape of the initial state. The best example of which is the relativistic isobaric collisions that the system uncertainties from the detectors and the bulk properties of the QGP medium can be largely canceled [37–40]. The correlations of the initial nucleons in the α cluster nuclei can also be probed by the correlations of the final particles in the heavy ion collisions. The STAR preliminary results already give some insight into the configuration of ^{16}O in relativistic ^{16}O + ^{16}O collisions [32].

Recently, tremendous efforts have been made to investigate the effect of α cluster on the flow harmonics and other observables in ^{16}O + ^{16}O collisions with the initial geometry models, the hydrodynamic models and the transport models [25–34]. Most of these studies focus on a typical configuration of α clusters in ^{16}O, obtained by nuclear structure theories or simple geometric constructions. However, due to different Hamiltonians and/or approximations, calculations such as variational Monte Carlo (VMC), nuclear lattice effective field theory (NLEFT), and extended quantum molecular dynamics (EQMD) give very different tetrahedral-like clustering correlations [6,23,41–43]. These different structures lead to different predictions on the observables of relativistic ^{16}O + ^{16}O collisions [32]. We find that these different predictions may be due to the compactness of the α cluster in ^{16}O—there could be a loose or compact "α" in the nuclei, compared to the size of free α nuclei ($r_\alpha \equiv \sqrt{\langle r^2 \rangle} = 1.71$ fm). In this work, we will use a state-of-the-art relativistic hydrodynamic model to study the effect of tetrahedral α cluster configurations on the final observables of ^{16}O + ^{16}O collisions at $\sqrt{s_{NN}} = 6.5$ TeV.

Model and setups. The dynamic evolution of the QGP medium created by the ^{16}O + ^{16}O collisions at $\sqrt{s_{NN}} = 6.5$ TeV is simulated by an `iEBE-VISHNU` [44,45] model. The `iEBE-VISHNU` is an event-by-event hybrid model that combines the `TRENTo` model generating the initial stage [46,47], the `VISH2+1` describing the collective expansion of the QGP [48–50], and the `UrQMD` [51,52] simulating the evolution of

*haojiexu@zjhu.edu.cn
†huichaosong@pku.edu.cn

TABLE I. The `iEBE-VISHNU` parameters for the simulation of $^{16}\mathrm{O}+^{16}\mathrm{O}$ collisions at $\sqrt{s_{NN}} = 6.5$ TeV. A detailed description of these parameters can be found Refs. [31,58].

Initial condition/Pre-eq.		QGP medium	
Norm	17 GeV	$(\eta/s)_{\min}$	0.11
p	0.0	$(\eta/s)_{\mathrm{slope}}$	1.6 GeV^{-1}
σ_{flut}	1.6	$(\eta/s)_{\mathrm{crv}}$	−0.29
r_{cp}	0.51 fm	$(\zeta/s)_{\max}$	0.032
n_{c}	1	$(\zeta/s)_{\mathrm{width}}$	0.024 GeV
w_{c}	0.51 fm	$(\zeta/s)_{T_0}$	0.175 GeV
$d_{\min}$	0.4 fm	T_{switch}	0.151 GeV
τ_{fs}	0.37 fm/c		

the hadron cascade in the hadronic rescattering process. All the model parameters are listed in Table I, except those for the structure of ^{16}O. With these parameters, the anisotropic flow observables measured by the ALICE and CMS collaborations [53–55] can be well described with our `iEBE-VISHNU` simulations.

In this Letter, we only focus on the tetrahedral configurations of α clusters in ^{16}O, but with more detailed discussions on the compactness of the α in the nuclei. Some other configurations such as linear chain and Y-shape configurations are also of interest but are beyond the scope of this study. In the tetrahedral configurations, the shape of oxygen is described by a tetrahedron of side length l, and the centers of four α clusters are placed at the vertices of the tetrahedron. The spatial coordinates of the nucleons in each α cluster are sampled from a three-dimensional (3D) Gaussian distribution with root-mean-square radius r_α, which describes the mean radius of each cluster. The r_α parameter reflects the compactness of the α cluster in the nuclei. A smaller r_α indicates a denser cluster in the nuclei. In this study, the nuclear density of ^{16}O is constructed with three magnitudes of r_α to comprehensively understand the effect of α cluster configurations on the final observables. We enforce that the root-mean-square radius of ^{16}O should be the same for the different densities ($\sqrt{\langle r^2\rangle} \equiv \sqrt{3l^2/8 + r_\alpha^2} = 2.73$ fm from the nuclear structure experiment [56], here, we ignore the differences between charge density and nuclear mass density), a large l is being required for the case of compacted α cluster. For comparison, a three parameter Fermi distribution (3pF) with the same root-mean-square radius of ^{16}O is also computed, $\rho = \rho_0(1 + \omega r^2/R^2)[1 + \exp((r - R)/a)]^{-1}$, where $R = 2.608$ fm, $a = 0.513$ fm, $\omega = -0.051$ fm [56]. The corresponding parameters are listed in Table II and the two-dimensional densities obtained by integrating their nuclear densities along one of their C3 rotation axes are shown in Fig. 1. Obvious triangular hot spots appear at small r_α/l. The one-body density $\rho(r)$ was enhanced at $r \sim 2$ fm with small r_α/l, consistent with recent study [57]. We find that the two-body correlation functions $C(r)$ [26] imply attractive effect at low separations r with small r_α/l, this needs to be further investigated with more realistic nuclear structure theory calculations.

We simulate ∼50 k hydrodynamic events of $^{16}\mathrm{O}+^{16}\mathrm{O}$ collisions at $\sqrt{s_{NN}} = 6.5$ TeV for each nuclear density at

TABLE II. The parameters (side length l of tetrahedron, the rms radius r_α of each cluster) for the nuclear distributions of ^{16}O with tetrahedral configurations of α clusters. The parameters for the Woods-Saxon distribution is $R = 2.608$ fm, $a = 0.513$ fm, and $\omega = -0.051$ fm [56].

	Distribution	l	r_α	r_α/l
I	Woods-Saxon			
II	α cluster	3.0	2.0	0.67
III	α cluster	3.6	1.6	0.44
IV	α cluster	4.0	1.2	0.30

the top 50% centrality, together with 2000 oversamplings of `UrQMD` afterburner for each hydrodynamic event. The centrality is determined by the charged particle multiplicity with $|\eta| < 0.5$. Based on these simulations, we find that several observables are sensitive to the configurations of ^{16}O, such as the mean transverse momenta $\langle p_{\mathrm{T}}\rangle \equiv \langle [p_{\mathrm{T}}]\rangle$, the two-particle $[p_{\mathrm{T}}]$ correlator $\langle \Delta p_{\mathrm{T}_i} \Delta p_{\mathrm{T}_j}\rangle$, the intensive skewness of $[p_{\mathrm{T}}]$ correlator $\Gamma_{p_{\mathrm{T}}}$, the elliptic flows $v_2\{2\}$, $v_2\{4\}$ and their ratios, the triangular flow $v_3\{2\}$, as well as the $v_n^2 - \delta[p_{\mathrm{T}}]$ correlations $\rho(v_2^2, [p_{\mathrm{T}}])$ and $\rho(v_3^2, [p_{\mathrm{T}}])$. Here, $[p_{\mathrm{T}}]$ is the mean transverse momentum of a given event and $\langle\cdots\rangle$ denotes the average over the ensemble of events.

Before the discussion of the results, some definitions of these observables are given below. The intensive skewness is defined by [59]

$$\Gamma_{p_{\mathrm{T}}} = \frac{\langle \Delta p_{\mathrm{T}_i} \Delta p_{\mathrm{T}_j} \Delta p_{\mathrm{T}_k}\rangle \langle p_{\mathrm{T}}\rangle}{\langle \Delta p_{\mathrm{T}_i} \Delta p_{\mathrm{T}_j}\rangle^2}. \tag{1}$$

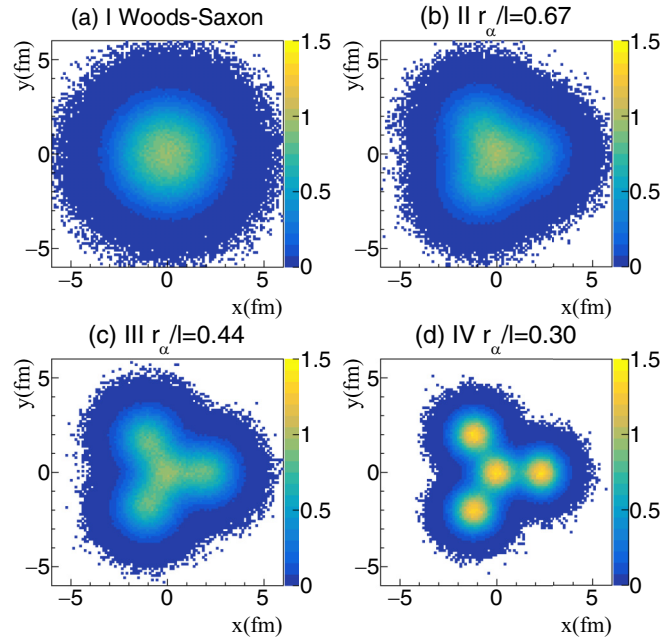

FIG. 1. The two-dimensional density distributions (unit in fm^{-2}) of the different tetrahedral configurations of ^{16}O listed in Table II, obtained by integrating their nuclear densities along one of their C3 rotation axes.

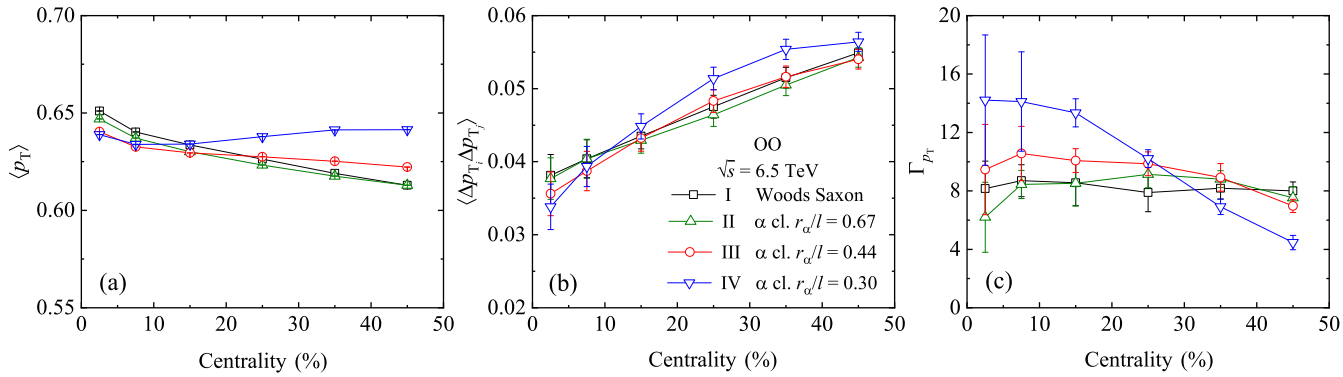

FIG. 2. The centrality dependent (a) mean transverse momenta $\langle p_T \rangle$, (b) two-particle $[p_T]$ correlator $\langle \Delta p_{T_i} \Delta p_{T_j} \rangle$, and (c) intensive skewness of $[p_T]$ correlator Γ_{p_T} of charged hadrons in $^{16}O + ^{16}O$ collisions at $\sqrt{s_{NN}} = 6.5$ TeV, calculated by the iEBE-VISHNU model with different initial state α cluster configurations.

Here, $\langle \Delta p_{T_i} \Delta p_{T_j} \rangle$ and $\langle \Delta p_{T_i} \Delta p_{T_j} \Delta p_{T_k} \rangle$ are the two- and three-particle correlators of $[p_T]$, defined as

$$\langle \Delta p_{T_i} \Delta p_{T_j} \rangle = \left\langle \frac{Q_1{}^2 - Q_2}{N_{ch}(N_{ch}-1)} \right\rangle - \left\langle \frac{Q_1}{N_{ch}} \right\rangle^2, \tag{2}$$

$$\langle \Delta p_{T_i} \Delta p_{T_j} \Delta p_{T_k} \rangle = \left\langle \frac{Q_1{}^3 + 2Q_3 - 3Q_1Q_2}{(N_{ch}-1)(N_{ch}-2)} \right\rangle + 2\left\langle \frac{Q_1}{N_{ch}} \right\rangle^3 - 3\left\langle \frac{Q_1}{N_{ch}} \right\rangle \left\langle \frac{Q_1{}^2 - Q_2}{N_{ch}(N_{ch}-1)} \right\rangle \tag{3}$$

with $Q_n = \sum_{i=1}^{N_{ch}} p_{T,i}^n$.

The Pearson correlation coefficient of $v_n^2 - \delta[p_T]$ correlation is defined by [60]

$$\rho\left(v_n^2, [p_T]\right) = \frac{\langle v_n^2 \delta[p_T] \rangle}{\sqrt{\langle (\delta v_n^2)^2 \rangle \langle (\delta[p_T])^2 \rangle}}, \tag{4}$$

which is an observable that sensitive to the initial geometry and its fluctuations. The associated flow harmonics are calculated with the Q-cumulant method [61].

Results and discussions. For our hydrodynamic simulations, the centrality cuts are slightly different with different ^{16}O densities. However, for the observables discussed in this study, the bias due to centrality cut differences are negligible when comparing the four cases. Quantitatively, most of the results discussed in this work can be described by the related initial predictors, i.e., $[p_T] \propto d_\perp \equiv E/S$ and $v_n \propto \epsilon_n$ [62,63]. Here, E and S are the initial total energy and entropy, and ϵ_n are the initial eccentricities.

Figure 2 shows the centrality dependent cumulants of the $\langle p_T \rangle$ distributions. Except for the very compact cluster in case IV, the predictions of these cumulants are roughly overlap within error bars. In relativistic heavy ion collisions, the $\langle p_T \rangle$ depends on the density of the overlap region [64,65], and the magnitude typically decreases with centrality, as in cases I–III shown in Fig. 2(a). However, when the α cluster is highly compact in the nuclei, as in case IV, there is a nonmonotonic centrality dependence for the $\langle p_T \rangle$, as the compact cluster reduces the $\langle p_T \rangle$ for central collisions and increases it for peripheral collisions. The effect of α configurations on two-particle $[p_T]$ correlator $\langle \Delta p_{T_i} \Delta p_{T_j} \rangle$ shown in Fig. 2(b) is similar to the $\langle p_T \rangle$, except that all trends show the correlator increasing with centrality. Conversely, the compact α cluster increases the intensity of the $[p_T]$ correlator Γ_{p_T} at central collisions and decreases it at peripheral collisions, see Fig. 2(c). The centrality dependence of Γ_{p_T} is weak for the first three cases of nuclear densities, while its prediction from case IV nuclear density shows a very obvious centrality dependence, the value decreasing with centrality. The effect of α cluster on the flow observables in $^{16}O + ^{16}O$ collisions are shown in Figs. 3 and 4. Such effect has been studied extensively in previous work. However, different studies give different conclusions on the α cluster effect. Some of them predicted that the effect of α cluster on flow observables is considerably small [31,32], while some other studies indicate that the flow observables can be used to detect the α cluster in oxygen [26,28,32]. This may be due to the different configurations used in their models. Here, we give a possible way to understand these differences.

Figure 3 shows the centrality dependent $v_2\{2\}$, $v_2\{4\}$ and their ratios in $^{16}O + ^{16}O$ collisions at $\sqrt{s_{NN}} = 6.5$ TeV, calculated from iEBE-VISHNU with different α cluster configurations.[1] The predictions from the Woods-Saxon density (case I) and the loose cluster density (case II) are similar. The reason is that with the large r_α/l in case II, the four α clusters in oxygen overlap with each other, and we get a smooth nuclear density as in the Woods-Saxon case. The compact α (case IV), however, introduces more fluctuations into the initial state, giving very different predictions for the centrality dependent elliptic flow. Especially for mid-center collisions like 10–30 % centralities, the enhancements of $v_2\{2\}$ and $v_2\{4\}$ due to the compact cluster in oxygen are obvious. An interesting feature is that such enhancements are larger for the elliptical flow obtained from four-particle correlations than those from two-particle correlations, resulting in non-trivial centrality dependent $v_2\{4\}/v_2\{2\}$ ratios, as shown in Fig. 3(c).

For flow observables in a single collision system, their individual magnitude depends on the properties of the QGP

[1] $c_2\{4\}$ tunes to positive value in the 40–50 % centrality, there thus is no $v_2\{4\} \equiv (-c_2\{4\})^{1/4}$ value above 40–50 % centrality for case IV in Figs. 3(b) and 3(c).

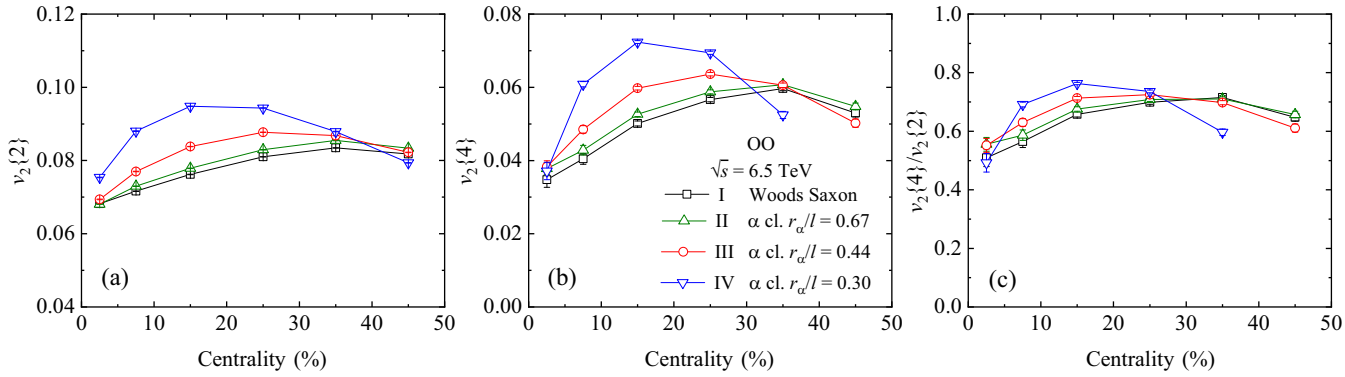

FIG. 3. The centrality dependent (a) $v_2\{2\}$, (b) $v_2\{4\}$, and (c) their ratios of all charged hadrons in $^{16}\mathrm{O}+^{16}\mathrm{O}$ collisions at $\sqrt{s_{NN}} = 6.5$ TeV, calculated by the iEBE-VISHNU model.

medium, we therefore prefer to discuss their ratios to explore the nuclear structure effect [39,66]. The $v_2\{4\}/v_2\{2\}$ have been used to study the α configurations in heavy ion experiments. In comparison to the initial model simulations, the STAR preliminary results on the centrality dependent $v_2\{4\}/v_2\{2\}$ ratio in central collisions are consistent with the prediction with α configuration from VMC calculations, while the prediction with α configuration from NLEFT calculations somehow failed. Based on our study with hydrodynamic simulations, the different predictions on the trends of the centrality dependent $v_2\{4\}/v_2\{2\}$ ratios are due to the different r_α/l under tetrahedral α configurations, the hydrodynamic simulations with a smaller r_α/l predict a rapid increase at the top 10% centrality. From nuclear structure theories, we know that the effective r_α/l from VMC is smaller than the one from NLEFT [6,23], consistent with our conclusions. Our study of the top RHIC energy is ongoing.

Figure 4 shows the centrality dependent triangular flow $v_3\{2\}$ in $^{16}\mathrm{O}+^{16}\mathrm{O}$ collisions at $\sqrt{s_{NN}} = 6.5$ TeV, calculated by iEBE-VISHNU model. The effect of the α cluster on $v_3\{2\}$ is obvious in the most central collisions. As mentioned above,

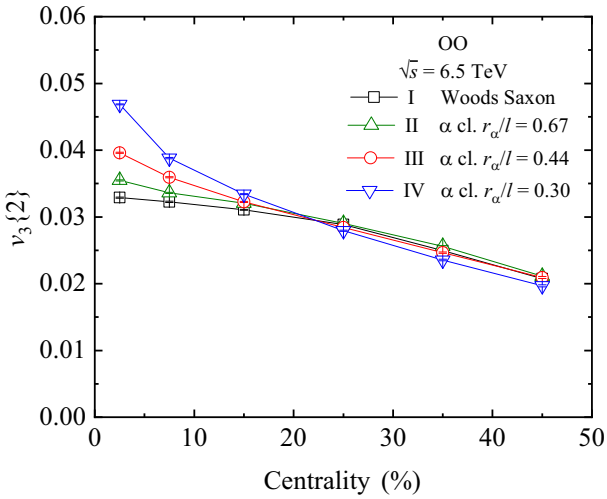

FIG. 4. The centrality dependent $v_3\{2\}$ of all charged hadrons in $^{16}\mathrm{O}+^{16}\mathrm{O}$ collisions at $\sqrt{s_{NN}} = 6.5$ TeV, calculated by the iEBE-VISHNU model.

the compact α cluster contributes large fluctuations to the initial profiles. However, one would expect such an effect to introduce some enhancement of the $v_3\{2\}$ for the whole centrality range. Therefore, the only enhancement at most central collisions shown in Fig. 4 is most likely due to the geometry becoming dominant contributions. We know that a large octupole deformation is an enhancement of $v_2\{2\}$ in midcentral collisions and $v_3\{2\}$ in most-central collisions [67], which is similar to the effect of the α clusters shown in Figs. 3 and 4. In fact, the cluster structure in oxygen indicates finite Q_{3X} with octupole deformation [68]. If we project the density into the transverse plane of the heavy ion collisions, we get an obvious triangular structure like the Hoyle $^{12}\mathrm{C}$, as shown in Fig. 1. Therefore, a nonzero β_3 would be required to parametrize the clustered oxygen with the Woods-Saxon formula, and it is interesting to further investigate the differences between the clustered density and its Woods-Saxon parametrization.

We now focus on the correlations between the two observables. Figure 5 shows the centrality dependent Pearson correlation coefficients $\rho(v_2^2, [p_\mathrm{T}])$ and $\rho(v_3^2, [p_\mathrm{T}])$, calculated by the iEBE-VISHNU model with different initial state α configurations. The $\rho(v_2^2, [p_\mathrm{T}])$ decreases and changes from positive to negative with respect to centrality, and it decreases faster in the configurations with compact α cluster. The $\rho(v_3^2, [p_\mathrm{T}])$ has negative correlations in all centralities with different nuclear densities, and it gains a strong suppression from the compact α cluster in oxygen. We note that the contributions of the α cluster to $\rho(v_2^2, [p_\mathrm{T}])$ have significant centrality dependence, while their contributions to $\rho(v_3^2, [p_\mathrm{T}])$ are weakly dependent on centrality. We therefore propose that the Pearson correlation coefficients $\rho(v_2^2, [p_\mathrm{T}])$ and $\rho(v_3^2, [p_\mathrm{T}])$ are sensitive observables to probe the compactness of α cluster in oxygen with relativistic heavy ion collisions.

Conclusion. Using the iEBE-VISHNU hybrid model, we have studied the effect of α clusters in $^{16}\mathrm{O}$ on the soft hadron observables in $^{16}\mathrm{O}+^{16}\mathrm{O}$ collisions at $\sqrt{s_{NN}} = 6.5$ TeV. We found that the importance of the α cluster for the observables in $^{16}\mathrm{O}+^{16}\mathrm{O}$ collisions depends on the compactness of the α cluster (i.e., r_α/l) in the light nuclei: densities with compact cluster (small r_α/l) give very different predictions from those of the Woods-Saxon density. The intensive skewness of the $[p_\mathrm{T}]$ correlator Γ_{p_T}, the elliptic flow $v_2\{2\}$, $v_2\{4\}$, and their

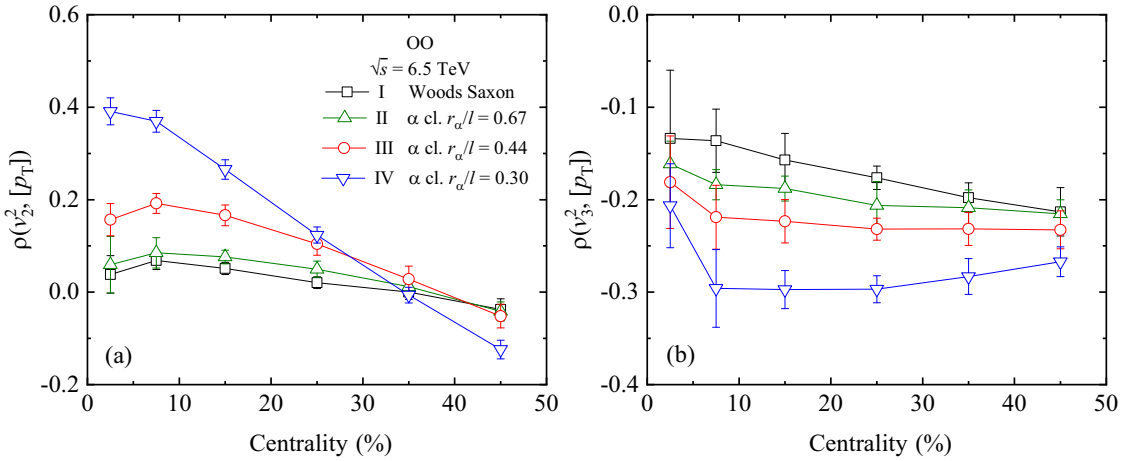

FIG. 5. The charged hadron Pearson correlation coefficients (a) $\rho(v_2^2, [p_T])$ and (b) $\rho(v_3^2, [p_T])$ as a function of centrality in $^{16}O + ^{16}O$ collisions at $\sqrt{s_{NN}} = 6.5$ TeV, calculated by the `iEBE-VISHNU` model.

ratios, the triangular flow $v_3\{2\}$, the Pearson correlation coefficients $\rho(v_2^2, [p_T])$ and $\rho(v_3^2, [p_T])$ are sensitive to r_α/l. The α cluster effect depends on the compactness of the α cluster in the ^{16}O, providing a possible way to explain the differences in previous predictions with the EQMD density and the NLEFT density. The magnitude of r_α/l reflects the properties of the strong interaction in a nucleus, which can give us some detailed information about QCD. We note that for a quantitative exploration of the compactness of α clusters in ^{16}O with heavy ion collisions, more effects such as the detailed distributions of each α cluster, the subnucleon structure, need to be further investigated. Therefore, our study serves as an important step towards a quantitative exploration of the compactness of the α cluster in light nuclei in relativistic heavy ion collisions. We expect that the value r_α/l can be extracted from our proposed observables in the current and upcoming relativistic $^{16}O + ^{16}O$ collision program at RHIC and the LHC.

Acknowledgments. We thanks S. Huang J. Jia, B. Lu, and X. Wang for useful discussions. This work is supported in part by the National Natural Science Foundation of China under Grants No. 12247107 and No. 12075007, H.J.X. is supported by the National Natural Science Foundation of China under Grants No. 12275082, No. 12035006, and No. 12075085.

[1] G. Gamow, *Constitution of Atomic Nuclei and Radioactivity* (Clarendon Press, Oxford, 1931).
[2] F. Hoyle, On nuclear reactions occuring in very hot stars. 1. The synthesis of elements from carbon to nickel, Astrophys. J. Suppl. Ser. **1**, 121 (1954).
[3] C. W. Cook, W. A. Fowler, C. C. Lauritsen, and T. Lauritsen, B^{12}, C^{12}, and the red giants, Phys. Rev. **107**, 508 (1957).
[4] D. N. F. Dunbar, R. E. Pixley, W. A. Wenzel, and W. Whaling, The 7.68-Mev state in C^{12}, Phys. Rev. **92**, 649 (1953).
[5] K. Ikeda, N. Takigawa, and H. Horiuchi, The systematic structure-change into the molecule-like structures in the self-conjugate 4*n* nuclei, Prog. Theor. Phys. Suppl. **E68**, 464 (1968).
[6] E. Epelbaum, H. Krebs, T. A. Lähde, D. Lee, Ulf.-G. Meißner, and G. Rupak, *Ab initio* calculation of the spectrum and structure of ^{16}O, Phys. Rev. Lett. **112**, 102501 (2014).
[7] T. A. Lähde, E. Epelbaum, H. Krebs, D. Lee, U.-G. Meißner, and G. Rupak, Lattice effective field theory for medium-mass nuclei, Phys. Lett. B **732**, 110 (2014).
[8] R. Bijker and F. Iachello, Evidence for tetrahedral symmetry in ^{16}O, Phys. Rev. Lett. **112**, 152501 (2014).
[9] R. Bijker and F. Iachello, The algebraic cluster model: Structure of ^{16}O, Nucl. Phys. A **957**, 154 (2017).
[10] Y. Kanada-En'yo, Structure of ground and excited states of ^{12}C, Prog. Theor. Phys. **117**, 655 (2007); The structure of ground and excited states of ^{12}C, **121**, 895(E) (2009).
[11] D. Dell'Aquila *et al.*, High precision probe of the fully sequential decay width of the Hoyle state in ^{12}C, Phys. Rev. Lett. **119**, 132501 (2017).
[12] R. Smith, T. Kokalova, C. Wheldon, J. E. Bishop, M. Freer, N. Curtis, and D. J. Parker, New measurement of the direct 3α decay from the ^{12}C Hoyle state, Phys. Rev. Lett. **119**, 132502 (2017).
[13] J. A. Wheeler, Molecular viewpoints in nuclear structure, Phys. Rev. **52**, 1083 (1937).
[14] K. Wildermuth and T. Kanellopoulos, The "cluster model" of the atomic nuclei, Nucl. Phys. **7**, 150 (1958).
[15] A. Tohsaki, H. Horiuchi, P. Schuck, and G. Ropke, Alpha cluster condensation in ^{12}C and ^{16}O, Phys. Rev. Lett. **87**, 192501 (2001).
[16] H. Feldmeier, Fermionic molecular dynamics Nucl. Phys. A **515**, 147 (1990).
[17] A. Ono, H. Horiuchi, T. Maruyama, and A. Ohnishi, Antisymmetrized version of molecular dynamics with two nucleon collisions and its application to heavy ion reactions, Prog. Theor. Phys. **87**, 1185 (1992).
[18] P. Navratil, J. P. Vary, and B. R. Barrett, Large basis *ab initio* no-core shell model and its application to ^{12}C, Phys. Rev. C **62**, 054311 (2000).
[19] F. Coester, Bound states of a many-particle system, Nucl. Phys. **7**, 421 (1958).

[20] H. Kummel, K. H. Luhrmann, and J. G. Zabolitzky, Many-Fermion theory in expS- (or coupled cluster) form, Phys. Rep. **36**, 1 (1978).

[21] W. Broniowski and E. Ruiz Arriola, Signatures of α clustering in light nuclei from relativistic nuclear collisions, Phys. Rev. Lett. **112**, 112501 (2014).

[22] S. Zhang, Y. G. Ma, J. H. Chen, W. B. He, and C. Zhong, Nuclear cluster structure effect on elliptic and triangular flows in heavy-ion collisions, Phys. Rev. C **95**, 064904 (2017).

[23] M. Rybczyński, M. Piotrowska, and W. Broniowski, Signatures of α clustering in ultrarelativistic collisions with light nuclei, Phys. Rev. C **97**, 034912 (2018).

[24] C.-C. Guo, Y.-G. Ma, Z.-D. An, and B.-S. Huang, Influence of α-clustering configurations in $^{16}\mathrm{O}+{}^{197}\mathrm{Au}$ collisions at Fermi energy, Phys. Rev. C **99**, 044607 (2019).

[25] S. H. Lim, J. Carlson, C. Loizides, D. Lonardoni, J. E. Lynn, J. L. Nagle, J. D. Orjuela Koop, and J. Ouellette, Exploring new small system geometries in heavy ion collisions, Phys. Rev. C **99**, 044904 (2019).

[26] M. Rybczyński and W. Broniowski, Glauber Monte Carlo predictions for ultrarelativistic collisions with $^{16}\mathrm{O}$, Phys. Rev. C **100**, 064912 (2019).

[27] Y.-Z. Wang, S. Zhang, and Y.-G. Ma, System dependence of away-side broadening and α-clustering light nuclei structure effect in dihadron azimuthal correlations, Phys. Lett. B **831**, 137198 (2022).

[28] Y.-A. Li, S. Zhang, and Y.-G. Ma, Signatures of α-clustering in $^{16}\mathrm{O}$ by using a multiphase transport model, Phys. Rev. C **102**, 054907 (2020).

[29] D. Behera, N. Mallick, S. Tripathy, S. Prasad, A. N. Mishra, and R. Sahoo, Predictions on global properties in O+O collisions at the Large Hadron Collider using a multi-phase transport model, Eur. Phys. J. A **58**, 175 (2022).

[30] C. Ding, L.-G. Pang, S. Zhang, and Y.-G. Ma, Signals of α clusters in $^{16}\mathrm{O}+{}^{16}\mathrm{O}$ collisions at the LHC from relativistic hydrodynamic simulations, Chin. Phys. C **47**, 024105 (2023).

[31] N. Summerfield, B.-N. Lu, C. Plumberg, D. Lee, J. Noronha-Hostler, and A. Timmins, $^{16}\mathrm{O}$ $^{16}\mathrm{O}$ collisions at energies available at the BNL Relativistic Heavy Ion Collider and at the CERN Large Hadron Collider comparing α clustering versus substructure, Phys. Rev. C **104**, L041901 (2021).

[32] S. Huang, Measurements of azimuthal anisotropies in $^{16}\mathrm{O}+{}^{16}\mathrm{O}$ and γ+Au collisions from STAR, arXiv:2312.12167.

[33] B. Schenke, C. Shen, and P. Tribedy, Running the gamut of high energy nuclear collisions, Phys. Rev. C **102**, 044905 (2020).

[34] G. Nijs and W. van der Schee, Predictions and postdictions for relativistic lead and oxygen collisions with the computational simulation code TRAJECTUM, Phys. Rev. C **106**, 044903 (2022).

[35] L.-M. Liu, S.-J. Li, Z. Wang, J. Xu, Z.-Z. Ren, and X.-G. Huang, Probing configuration of α clusters with spectator particles in relativistic heavy-ion collisions, arXiv:2312.13572.

[36] J. Brewer, A. Mazeliauskas, and W. van der Schee, Opportunities of OO and pO collisions at the LHC, arXiv:2103.01939.

[37] H. Li, H.-J. Xu, Y. Zhou, X. Wang, J. Zhao, L.-W. Chen, and F. Wang, Probing the neutron skin with ultrarelativistic isobaric collisions, Phys. Rev. Lett. **125**, 222301 (2020).

[38] H.-j. Xu, H. Li, X. Wang, C. Shen, and F. Wang, Determine the neutron skin type by relativistic isobaric collisions, Phys. Lett. B **819**, 136453 (2021).

[39] H.-J. Xu, W. Zhao, H. Li, Y. Zhou, L.-W. Chen, and F. Wang, Probing nuclear structure with mean transverse momentum in relativistic isobar collisions, Phys. Rev. C **108**, L011902 (2023).

[40] S. Zhao, H.-j. Xu, Y.-X. Liu, and H. Song, Probing the nuclear deformation with three-particle asymmetric cumulant in RHIC isobar runs, Phys. Lett. B **839**, 137838 (2023).

[41] S. C. Pieper, K. Varga, and R. B. Wiringa, Quantum Monte Carlo calculations of A = 9, 10 nuclei, Phys. Rev. C **66**, 044310 (2002).

[42] D. Lee, Lattice simulations for few- and many-body systems, Prog. Part. Nucl. Phys. **63**, 117 (2009).

[43] W. B. He, Y. G. Ma, X. G. Cao, X. Z. Cai, and G. Q. Zhang, Giant dipole resonance as a fingerprint of α clustering configurations in $^{12}\mathrm{C}$ and $^{16}\mathrm{O}$, Phys. Rev. Lett. **113**, 032506 (2014).

[44] C. Shen, Z. Qiu, H. Song, J. Bernhard, S. Bass, and U. Heinz, The IEBE-VISHNU code package for relativistic heavy-ion collisions, Comput. Phys. Commun. **199**, 61 (2016).

[45] H. Song, S. A. Bass, and U. Heinz, Viscous QCD matter in a hybrid hydrodynamic+Boltzmann approach, Phys. Rev. C **83**, 024912 (2011).

[46] J. S. Moreland, J. E. Bernhard, and S. A. Bass, Alternative ansatz to wounded nucleon and binary collision scaling in high-energy nuclear collisions, Phys. Rev. C **92**, 011901(R) (2015).

[47] J. E. Bernhard, J. S. Moreland, S. A. Bass, J. Liu, and U. Heinz, Applying Bayesian parameter estimation to relativistic heavy-ion collisions: Simultaneous characterization of the initial state and quark-gluon plasma medium, Phys. Rev. C **94**, 024907 (2016).

[48] U. W. Heinz, H. Song, and A. K. Chaudhuri, Dissipative hydrodynamics for viscous relativistic fluids, Phys. Rev. C **73**, 034904 (2006).

[49] H. Song and U. W. Heinz, Causal viscous hydrodynamics in 2+1 dimensions for relativistic heavy-ion collisions, Phys. Rev. C **77**, 064901 (2008).

[50] H. Song and U. W. Heinz, Suppression of elliptic flow in a minimally viscous quark-gluon plasma, Phys. Lett. B **658**, 279 (2008).

[51] S. A. Bass *et al.*, Microscopic models for ultrarelativistic heavy ion collisions, Prog. Part. Nucl. Phys. **41**, 255 (1998).

[52] M. Bleicher *et al.*, Relativistic hadron-hadron collisions in the ultrarelativistic quantum molecular dynamics model, J. Phys. G: Nucl. Part. Phys. **25**, 1859 (1999).

[53] J. Adam *et al.* (ALICE Collaboration), Centrality dependence of the charged-particle multiplicity density at midrapidity in Pb-Pb collisions at $\sqrt{s_{\mathrm{NN}}} = 5.02$ TeV, Phys. Rev. Lett. **116**, 222302 (2016).

[54] S. Chatrchyan *et al.* (CMS Collaboration), Multiplicity and transverse momentum dependence of two- and four-particle correlations in pPb and PbPb collisions, Phys. Lett. B **724**, 213 (2013).

[55] B. B. Abelev *et al.* (ALICE Collaboration), Multiplicity dependence of the average transverse momentum in pp, p-Pb, and Pb-Pb collisions at the LHC, Phys. Lett. B **727**, 371 (2013).

[56] H. De Vries, C. W. de Jager and C. de Vries, At. Data Nucl. Data Tables **36**, 495 (1987).

[57] G. Giacalone *et al.*, The unexpected uses of a bowling pin: exploiting $^{20}\mathrm{Ne}$ isotopes for precision characterizations of collectivity in small systems, arXiv:2402.05995 (2024).

[58] J. S. Moreland, J. E. Bernhard, and S. A. Bass, Bayesian calibration of a hybrid nuclear collision model using p-Pb and Pb-Pb

data at energies available at the CERN Large Hadron Collider, Phys. Rev. C **101**, 024911 (2020).
[59] G. Giacalone, F. G. Gardim, J. Noronha-Hostler, and J.-Y. Ollitrault, Skewness of mean transverse momentum fluctuations in heavy-ion collisions, Phys. Rev. C **103**, 024910 (2021).
[60] P. Bożek, Transverse-momentum–flow correlations in relativistic heavy-ion collisions, Phys. Rev. C **93**, 044908 (2016).
[61] A. Bilandzic, R. Snellings, and S. Voloshin, Flow analysis with cumulants: Direct calculations, Phys. Rev. C **83**, 044913 (2011).
[62] D. Teaney and L. Yan, Triangularity and dipole asymmetry in heavy ion collisions, Phys. Rev. C **83**, 064904 (2011).
[63] G. Giacalone, F. G. Gardim, J. Noronha-Hostler, and J.-Y. Ollitrault, Correlation between mean transverse momentum and anisotropic flow in heavy-ion collisions, Phys. Rev. C **103**, 024909 (2021).
[64] W. Broniowski, M. Chojnacki, and L. Obara, Size fluctuations of the initial source and the event-by-event transverse momentum fluctuations in relativistic heavy-ion collisions, Phys. Rev. C **80**, 051902(R) (2009).
[65] B. Schenke, C. Shen, and D. Teaney, Transverse momentum fluctuations and their correlation with elliptic flow in nuclear collision, Phys. Rev. C **102**, 034905 (2020).
[66] Q. Liu, S. Zhao, H.-j. Xu, and H. Song, Determining the neutron skin thickness by relativistic semi-isobaric collisions, Phys. Rev. C **109**, 034912 (2024).
[67] J. Jia, Shape of atomic nuclei in heavy ion collisions, Phys. Rev. C **105**, 014905 (2022).
[68] X. B. Wang, G. X. Dong, Z. C. Gao, Y. S. Chen, and C. W. Shen, Tetrahedral symmetry in the ground state of ^{16}O, Phys. Lett. B **790**, 498 (2019).